

Spin Signature of Majorana Fermions in Topological Nodal-Point Superconductors

Junjie Zeng,¹ James Jun He,^{2,3} Zhen Ning,¹ Dong-Hui Xu,^{1,4,*} and Rui Wang^{1,4,†}

¹*Institute for Structure and Function & Department of Physics & Chongqing Key Laboratory for Strongly Coupled Physics, Chongqing University, Chongqing 400044, P. R. China*

²*International Center for Quantum Design of Functional Materials (ICQD), Hefei National Research Center for Interdisciplinary Sciences at the Microscale, University of Science and Technology of China, Hefei, Anhui 230026, China*

³*Hefei National Laboratory, Hefei, Anhui 230088, China*

⁴*Center of Quantum materials and devices, Chongqing University, Chongqing 400044, P. R. China*

(Dated: June 6, 2024)

In two-dimensional topological nodal superconductors, Majorana edge states have been conventionally believed to exhibit only spin-triplet pairing correlations. However, we reveal a substantial spin-singlet pairing component in Majorana edge states of antiferromagnetic topological nodal-point superconductors. This unexpected phenomenon emerges from the interplay between antiferromagnetic order and symmetry, resulting in Majorana edge states with a nearly flat band dispersion, deviating from the strictly flat band. Crucially, this phenomenon is detectable through spin-selective Andreev reflection, where the zero-bias conductance peaks are maximized when the spin of incident electrons is nearly antiparallel to that of Majorana edge excitations. This discovery unveils a unique spin signature for Andreev reflection resonances, advancing our fundamental understanding of spin-dependent mechanisms in topological superconductivity and representing a significant step towards the experimental detection of Majorana fermions.

Introduction.—In recent years, topological superconductors have attracted significant attention as a canonical example of topological phases of matter which host exotic Majorana quasiparticles. Majorana zero modes (MZMs), exhibiting non-Abelian statistics, are predicted to exist in these systems—either as end states in one-dimensional (1D) topological superconductors or as vortex bound states in two-dimensional (2D) topological superconductors [1–4]. In addition to the fundamental physical interest, MZMs provide a practical avenue for information processing in future fault-tolerant quantum computers [5, 6] as well. Topological superconductors also exhibit Majorana modes bound to their 1D or 2D boundaries, enforced by the bulk-boundary correspondence. Moreover, beyond the gapped topological superconductors, gapless nodal superconductors with nontrivial topology are another class of topological phases accommodating Majorana boundary excitations which terminate at the projection of bulk nodes [7]. Topological nodal superconductors have been proposed in various superconducting materials with the need for unconventional Cooper pairing [8–11]. Meanwhile, artificial topological nodal superconductivity is predicted to be realized in hybrid systems with conventional s -wave pairing symmetry [12, 13]. A recent focus has centered on the realization of topological nodal superconductivity in hybrid systems by proximity-coupling antiferromagnetic (AFM) materials to s -wave superconductors [14–16]. Notably, antiferromagnets, devoid of a net magnetic moment, avoid significant exchange fields that could disrupt Cooper pairs. Very recently, 2D topological nodal-point superconductivity is experimentally reported in the AFM magnet/superconductor hybrid of Mn/Nb(110) by measuring low-temperature tunneling spectroscopy [17].

Whether Majorana quasiparticles have been conclusively detected is still an open and controversial question in experimental investigations of topological superconductors. One

of the most prominent features pertained to MZMs probably is the zero-bias conductance peaks (ZBCPs), from experiments of either scanning tunneling microscope measurements or transport processes in tunneling junctions. Therefore, many research works treat ZBCPs as the suggesting evidence for the occurrence of MZMs [18–28]. But whether a feature as ZBCPs adequately supports the existence of MZMs has not yet gained its full certainty, because the appearance of ZBCPs, can have other provenance, e.g., topologically trivial bound states [29–37].

On the other hand, MZMs leave unique fingerprints in spin-sensitive measurements [38–45], thus providing the means to distinguish them from trivial zero-energy states. The basic standing ground is that MZMs have spin-triplet pairing correlations [46, 47]. These pairing correlations can manifest in transport behaviors when the quasiparticles participate in Andreev reflection processes. Remarkably, MZM-induced spin-selective Andreev reflection was experimentally evidenced in detecting vortex core states of topological superconductivity in the topological insulator/superconductor heterostructures [41]. In 2D topological nodal superconductors, the Majorana edge modes with strictly flat bands are believed to exhibit spin-triplet pairing correlations due to numerous MZMs residing on the sample boundaries [48, 49]. Therefore, the spin-selective Andreev reflection induced by MZMs is also expected to appear in topological nodal superconductors. Considering that the topological nodal superconductivity with the AFM order is protected by the spatial-dependent symmetry, the spectrum features of Majorana edge modes would strongly depend on the edge geometry.

A natural question arises whether the interplay of AFM order and symmetry in topological nodal superconductors leads to exotic spin-resolved transport phenomena. In this Letter, we address this issue and uncover a previously overlooked scenario. We show that spin-singlet pairing correlations play

a significant role due to Majorana edge modes manifesting in nearly flat bands instead of strictly flat bands. Remarkably, the ZBCPs in Andreev reflection are now strongest when the spin polarization of incident electrons is antiparallel to that of Majorana edge modes. This challenges the widely-held belief that ZBCPs are most prominent when the spin polarizations of incident electrons and Majorana edge modes are (nearly) parallel. Our findings not only unveil a novel spin signature in topological superconductivity, but also further enhance the understanding of the spin-dependent mechanism of Majorana fermions with further theoretical and experimental implications.

Model and Basic Behavior in Andreev Reflection.—The topological nodal-point superconductivity coexisting with antiferromagnetism in a 2D rectangular bisublatticed system [as shown in Fig. 1(a)] is captured by the model [17, 50, 51]

$$\begin{aligned}
 H &= H_0 + H_{\text{RSOC}} + H_{\text{AFM}} + H_{\text{SC}}, \quad (1) \\
 H_0 &= \left(t \sum_{\langle ij \rangle} + t' \sum_{\langle\langle ij \rangle\rangle} + t'' \sum_{\langle\langle\langle ij \rangle\rangle\rangle} \right) c_i^\dagger \cdot c_j - \mu \sum_i c_i^\dagger \cdot c_i, \\
 H_{\text{RSOC}} &= it_{\text{R}} \sum_{\langle ij \rangle, \langle\langle ij \rangle\rangle} c_i^\dagger \cdot (\mathbf{s} \times \hat{\mathbf{n}}_{ij})_z \cdot c_j, \\
 H_{\text{AFM}} &= J \sum_i c_i^\dagger \cdot (e^{i\mathbf{x}_i \cdot \mathbf{Q} + i\pi/2} s_3) \cdot c_i, \\
 H_{\text{SC}} &= \Delta \sum_i c_{i\uparrow}^\dagger c_{i\downarrow}^\dagger + \text{H.c.},
 \end{aligned}$$

where the first term H_0 contains the chemical potential μ and hoppings up to the 3rd nearest neighbors; the second term H_{RSOC} is the Rashba spin-orbit coupling (RSOC) measured by the parameter t_{R} between sites from the 1st to the 2nd nearest neighbors, where $\hat{\mathbf{n}}_{ij}$ is the unit directional vector for the hopping from site j to site i ; the third term H_{AFM} depicts the antiferromagnetism with sublattice resolution with the vector \mathbf{Q} as either one of the reciprocal lattice vectors; and the last term H_{SC} is the conventional s -wave superconducting (SC) pairing with the amplitude Δ contributed from the substrate. $c_i^\dagger = (c_{i\uparrow}^\dagger, c_{i\downarrow}^\dagger)$ is the electron creation operator including spin at site i , and $\mathbf{s} = (s_1, s_2, s_3)$ is the spin Pauli matrices. The bulk Hamiltonian Eq. (1) obviously respects the particle-hole (charge conjugation) symmetry \mathcal{P} , i.e., $\mathcal{P}H(\mathbf{k})\mathcal{P}^{-1} = -H(-\mathbf{k})$. The AFM order explicitly breaks the time-reversal symmetry Θ ; however, a combined symmetry (or termed as an effective time-reversal symmetry) $\mathcal{S} = \Theta T_{1/2}$ is preserved, and here $T_{1/2} = e^{i\mathbf{k} \cdot (\mathbf{a}_1 + \mathbf{a}_2)/2}$ denotes the half-translation operator connecting nearest spin-up and spin-down magnetic atoms [see Fig. 1(a)]. This effective time-reversal symmetry \mathcal{S} is antiunitary with $\mathcal{S}^2 = -e^{i\mathbf{k} \cdot (\mathbf{a}_1 + \mathbf{a}_2)}$ and depends on the crystal structure. Moreover, by combining the particle-hole symmetry \mathcal{P} and effective time-reversal symmetry \mathcal{S} , we can define an AFM chiral symmetry as $\mathcal{C} = \mathcal{S}\mathcal{P}$, which constrains the bulk Hamiltonian Eq. (1) as $\mathcal{C}H(\mathbf{k})\mathcal{C}^{-1} = -H(\mathbf{k})$.

Since the AFM chiral symmetry \mathcal{C} possesses the crystalline nature, the Majorana edge modes in the AFM topological nodal superconductor are sensitive to edge geometries. When

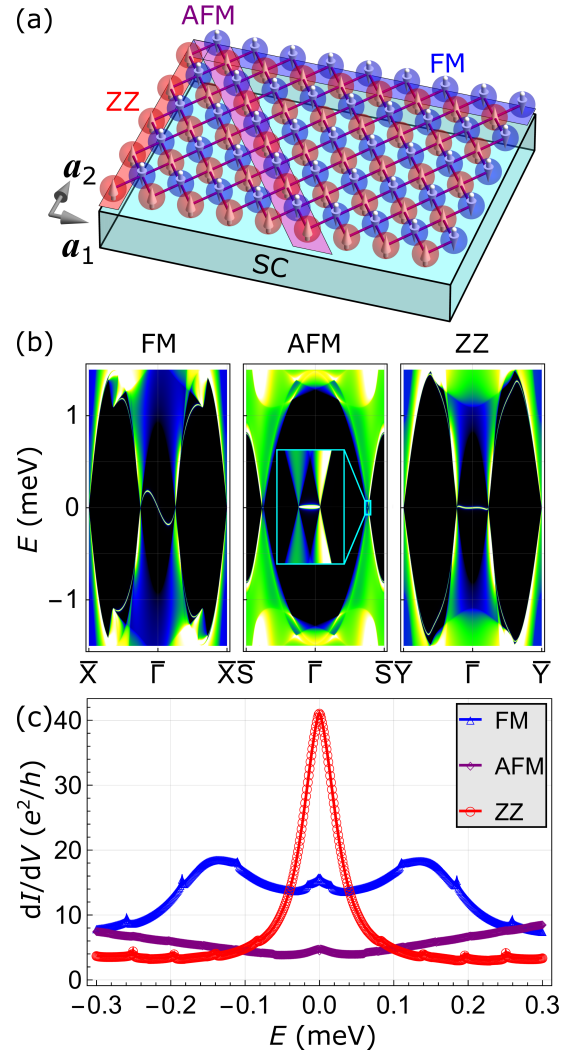


FIG. 1. Scenario of existence of the Majorana edge modes and their corresponding Andreev reflection behaviors. (a) Lattice structure of an AFM monolayer system on top of a conventional superconducting substrate, with lattice constants along the two orthogonal directions $|\mathbf{a}_2| = \sqrt{2}|\mathbf{a}_1| = \sqrt{2}$, if we chose $|\mathbf{a}_1| = 1$; the red and blue balls show the two sets of sublattices with opposite magnetic polarizations and connected by purple sticks are the 1st nearest neighbors; the three types of edges are labeled, respectively, by light blue, purple, and red background bands. (b) The existence of Majorana edge modes for each type of edge by the spectral function. (c) The ZZ edge mode gives rise to the most conspicuous peak signal in the process of Andreev reflection of a single-terminal tunneling junction.

the system terminates with a ribbon geometry along an appropriate crystallographic orientation, as shown in Fig. 1(a), three kinds of edges, i.e., the ferromagnetic (FM), AFM, and zigzag (ZZ) edges, can be formed. The FM and ZZ edges locally break \mathcal{C} , which is in contrast to the AFM edge with the \mathcal{C} protection. To reveal topological and transport properties of different edge geometries, we carried out the calculations of local density of states and the Andreev reflection. The values of all parameters in Eq. (1) are chosen to be the same as in

Ref. [17], and the technical details are included in the Supplemental Material (SM) [52]. The topological nodal-point superconducting phase and its Majorana edge modes related to different edges are reproduced as shown in Fig. S1 [52] and Fig. 1(b), respectively. It is found that these three edges host different Majorana edge modes in terms of degree of dispersiveness and the length spanned in the momentum space. The edge modes on the AFM edge are exactly flat [see the middle inset of Fig. 1(b)] and pinned to zero energy due to the preserved C . However, the projections of bulk nodes on the AFM edge are very close to each other due to the intrinsic structural features, so these flat-band Majorana edge modes only exist in a rather narrow wave vector window and do not give a ZBCP, as shown in Fig. 1(c). In contrast, the breaking of AFM chiral symmetry C leads to the emergence of dispersive Majorana edge modes appearing between the projections of bulk nodes. Remarkably, even with the breaking of C , the ZZ edge surprisingly hosts Majorana edge modes associated with a nearly flat band and a sizable width of wave vector window, indicating that a balance between a high density of states and finite group velocities can be achieved. When subjected to a weak coupling to a lead providing incident electrons, the nearly flat-band Majorana edge modes can develop an obvious ZBCP [colored red in Fig. 1(c)].

Pairing Correlation and Spin Polarization of Majorana Edge Modes.—As depicted above, the dispersion of Majorana edge modes strongly depends on edge geometries in the AFM topological nodal-point superconductor. Specifically, we notice that the nearly flat-band Majorana edge modes on the ZZ edge with breaking the AFM chiral symmetry C is actually dispersive, which corresponds to finite group velocities though at small magnitudes. Previously related researches all reported that the exactly flat-band Majorana edge modes are dominated by spin-triplet pairing correlations [48, 49]. Considering that the exactly flat band hosts the entirely zero group velocity but the nearly flat band exhibits a finite group velocity, it is expected that the Majorana edge modes associated with the nearly flat band can give rise to exotic effects. To further reveal this, we examine the pairing correlation of the Majorana edge modes in the present system. In this work, the spin (correlation and polarization) information is encoded in the linear combination coefficients d_s of spin Pauli matrices, extracted from the electron-hole block of the Green's function as $G_{\text{eh}} = (d_0 s_0 + \mathbf{d} \cdot \mathbf{s}) (i s_2)$ [53, 54] of a sheet system with a finite width along \mathbf{a}_2 but a semi-infinite length along \mathbf{a}_1 . Then the scalar and vector coefficients d_0 and \mathbf{d} represent, respectively, the amplitudes of spin-singlet and spin-triplet pairing correlations. The calculated results are displayed in Fig. 2. Panels (a)-(c) show the local magnitudes of both the spin-singlet ($|d_0|$) and triplet ($|\mathbf{d}|$) components for three typical energies ($E = 0$ meV, 0.03 meV, and 0.05 meV). One can see that among all the three cases, the spin-singlet component $|d_0|$ takes finite values all over the central region, but those near the edges are obviously larger than those in the bulk. Meanwhile, the two (ZZ and FM) edges yield mostly the same $|d_0|$ in magnitudes. On the other hand, the total spin-

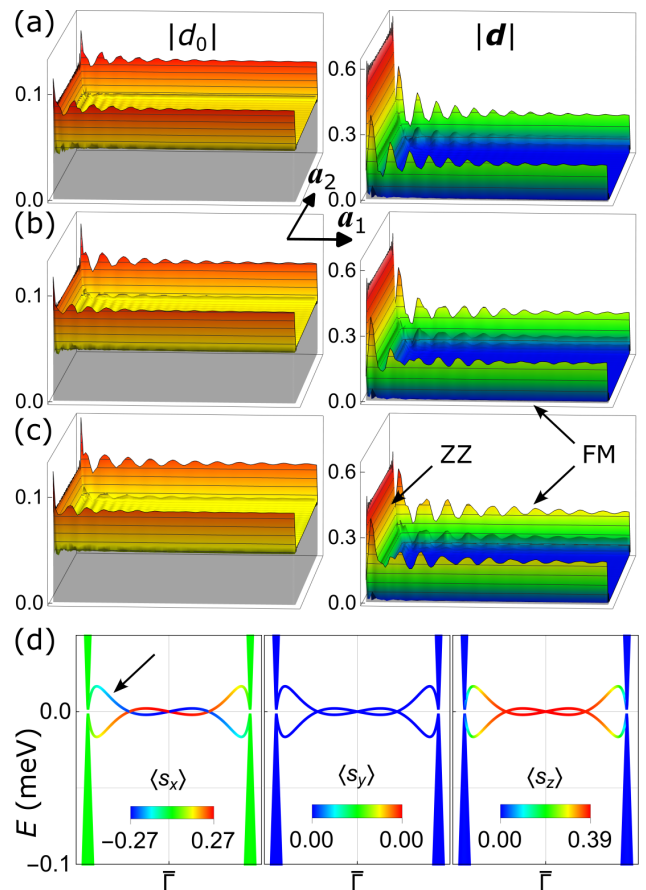


FIG. 2. Spin information for the Majorana edge modes. Pairing correlations of the ZZ and the FM Majorana edge modes: (a)-(c) Local spin-singlet $|d_0|$ (left) and total spin-triplet $|\mathbf{d}|$ (right) correlations for three typical energy values ($E = 0, 0.03$, and 0.05 meV) of the central region; dramatic difference between them does not exist. (d) Components of spin polarization for the pristine ZZ edge modes.

triplet component $|\mathbf{d}|$ shows a similar trend, except that now the bulk barely contribute and the values on the ZZ edge is much higher than those on the FM edge. More importantly, though smaller, $|d_0|$ is always of the same order of magnitude as $|\mathbf{d}|$, which is in sharp contrast to the situation of its exactly flat-band counterpart with the negligible spin-singlet pairing amplitude (see Sec. SII of the SM [52]). Moreover, as the energy increases, the spin-singlet pairing amplitude $|d_0|$ show slight increase and simultaneously the spin-triplet pairing amplitude $|\mathbf{d}|$ decreases obviously. That is to say, the spin-singlet component can show more prominent manifestations with the increase of energy. Additionally, as shown in Fig. 2(d), the left-upper branch of ZZ edge mode (indicated by the black arrow) bears a spin polarization of finite negative and positive components, respectively, in the x - and z -direction; but a vanishing one for s_y . Namely, around the zero energy this ZZ edge mode has a spin polarization with an acute polar angle and an azimuthal angle of the largest magnitude. Specifically, when the self energy modification of a probe lead is included, this ZZ edge mode would possess a spin polarization with the

orientation $(\theta_s, \phi_s) \approx (\pi/3, \pm\pi)$ (see the details in Sec. SIII of the SM [52]).

It is evident that the spin-singlet component of pairing correlation remains largely unsuppressed for the nearly flat-band Majorana edge modes on the ZZ edge. This contrasts significantly with previously studied systems with exactly flat-band Majorana edge modes, where the spin-singlet contribution is negligible compared with the spin-triplet component [48, 49]. The key to understanding this discrepancy lies in the AFM chiral symmetry of the system [17, 55]. While the 2D bulk model respects this symmetry, it is spatially dependent, meaning that introducing edges can disrupt it. The AFM chiral symmetry is conserved by the AFM edges, but is broken by the ZZ edges. The same information is embodied in Majorana edge modes that those for the AFM edge are flat but those for the latter become dispersive [Fig. 1(b)]. To verify this issue, we also change the parameters in Eq. (1) to enlarge the wave vector window of flat-band Majorana edge modes on the AFM edge. As expected, the results show that the spin-singlet pairing amplitude is also negligible (see Fig. S2 in the SM [52]).

Manifestation in Spin-Selective Andreev Reflection.—In the following, we show that the nearly flat-band Majorana edge modes have unique Andreev reflection features when the incident electrons are spin polarized, facilitating its experimental detection. To start with, we first let the electrons from a FM probe lead inject onto the ZZ edge of a central rectangular region, because the Majorana edge modes on the ZZ edge contribute to the most prominent ZBCP as shown in Fig. 1(c). The polarization of the incident electrons are characterized by the polar angle θ_J and the azimuthal angle ϕ_J , defined with respect to the directions of $(\mathbf{a}_1 \times \mathbf{a}_2)$ and \mathbf{a}_1 , respectively. The corresponding results are shown in Fig. 3(a). It is found that for a completely out-of-plane polarized spin, i.e., $\theta_J = 0$ (colored in red) or $\theta_J = \pi$ (colored in black), the change of ϕ_J makes no difference. And they can serve as the eye-guiders. Starting from the $\phi_J = 0$ case, one can see that the curve of $\theta_J = 2\pi/3$ (colored in blue) is above the one of $\theta_J = \pi$ (colored in black) and the one of $\theta_J = \pi/3$ (colored in green) lies below. The increase of the azimuthal angle pushes the blue and the green curves close to the lowest red one. The difference is that although both of them are decreasing overall, the height of the blue peak largely maintains, but the green peak reduces. More importantly, no matter how the azimuthal angle changes ($\phi_J \in [0, \pi/2]$), the highest and widest ZBCP always comes from some obtuse polar angles ($\theta_J = 2\pi/3, \pi$). Combining all the above messages with the spin polarization displayed in the previous section [see Fig. 2(d)], we find that when the spin polarization of the injecting electron in the probe lead is (approximately) opposite to that of the Majorana edge mode in the central scattering region, the heights and widths of the ZBCPs are maximized. Moreover, consistent behaviors from a half-metal probe lead are shown in Fig. 3(b), where the injection electrons are entirely spin polarized [56] (see Sec. SIII of the SM for adding magnetism into the probe lead [52]). Now although the maximal heights of the ZBCPs are slightly

smaller, the peaks are overall thinner in width, making them display more visual prominence. To summarize, our findings demonstrate that while the nearly flat-band Majorana edge modes on the ZZ edge lead to a wide ZBCP, the coexistence of spin-singlet and triplet components of the pairing correlation results in a spin-dependent Andreev reflection that deviates from that induced by the exactly flat-band Majorana edge modes protected by the AFM chiral symmetry C .

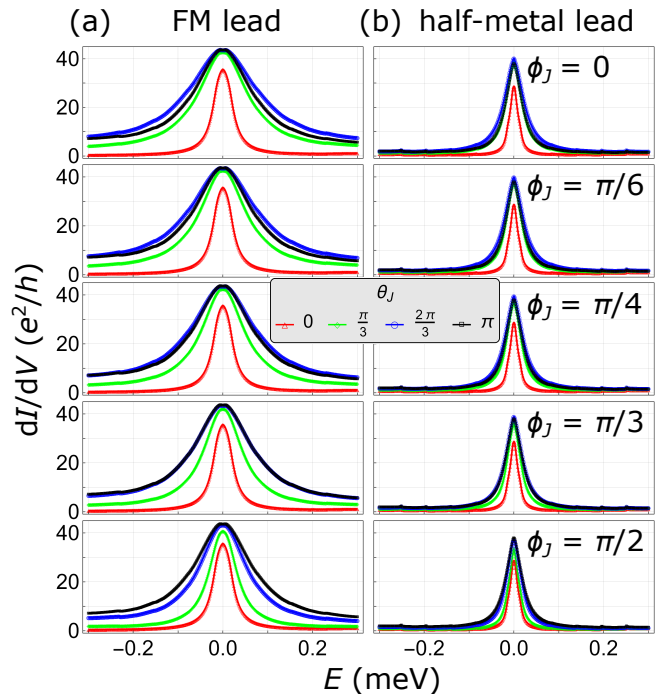


FIG. 3. Spin-dependent ZBCPs from the ZZ Majorana edge modes for (a) FM and (b) Half-metal probe lead. (θ_J, ϕ_J) specify the orientation of the spin polarization of the incident electron.

Summary and Discussion.—We investigated the spin characteristics of Majorana edge modes in a topological nodal-point superconductor with antiferromagnetism, where edge geometry and symmetry breaking significantly influence the spectrum features of Majorana edge modes. We discovered that breaking the antiferromagnetic chiral symmetry leads to non-negligible spin-singlet pairing correlations in nearly flat-band Majorana edge modes. This challenges the previous assumption that exactly flat-band Majorana edge modes in 2D topological nodal superconductors are solely dominated by spin-triplet pairing. Our finding hinges on the ability of nearly flat-band Majorana edge modes to balance high density of states with finite group velocities. Furthermore, we demonstrated unique spin-selective Andreev reflection behaviors in these Majorana edge modes.

Our results emphasize the importance of considering the potential manifestation of spin-singlet pairing correlations in transport processes like Andreev reflection, especially when the dispersion of Majorana edge states connecting bulk node projections deviates from strict flatness. This work contributes to a deeper understanding of the spin-dependent mechanisms

governing Majorana fermions.

Acknowledgement.—This work was supported by the National Natural Science Foundation of China (NSFC, Grants No. 1222402, No. 92365101, No. 12074108, and 12347101), the Chongqing Natural Science Foundation (Grants No. CSTB2023NSCQ-JQX0024 and No. CSTB2022NSCQ-MSX0568).

* donghuixu@cqu.edu.cn

† rcwang@cqu.edu.cn

- [1] A. Y. Kitaev, *Phys. Usp.* **44**, 131 (2001).
- [2] N. Read and D. Green, *Phys. Rev. B* **61**, 10267 (2000).
- [3] G. E. Volovik, *JETP Letters* **70**, 609 (1999).
- [4] D. A. Ivanov, *Phys. Rev. Lett.* **86**, 268 (2001).
- [5] A. Kitaev, *Ann. Phys.* **303**, 2 (2003).
- [6] C. Nayak, S. H. Simon, A. Stern, M. Freedman, and S. D. Sarma, *Rev. Mod. Phys.* **80**, 1083 (2008).
- [7] A. P. Schnyder and P. M. Brydon, *J. Phys. Condens. Matter* **27**, 243201 (2015).
- [8] M. Sato, *Phys. Rev. B* **73**, 214502 (2006).
- [9] S. A. Yang, H. Pan, and F. Zhang, *Phys. Rev. Lett.* **113**, 046401 (2014).
- [10] B. Béri, *Phys. Rev. B* **81**, 134515 (2010).
- [11] A. K. Nayak, A. Steinbok, Y. Roet, J. Koo, G. Margalit, I. Feldman, A. Almoalem, A. Kanigel, G. A. Fiete, B. Yan, Y. Oreg, N. Avraham, and H. Beidenkopf, *Nat. Phys.* **17**, 1413 (2021).
- [12] M. Sato and S. Fujimoto, *Phys. Rev. Lett.* **105**, 217001 (2010).
- [13] C. L. M. Wong, J. Liu, K. T. Law, and P. A. Lee, *Phys. Rev. B* **88**, 060504 (2013).
- [14] J. L. Lado and M. Sigrist, *Phys. Rev. Lett.* **121**, 037002 (2018).
- [15] W. Brzezicki and M. Cuoco, *Phys. Rev. B* **97**, 064513 (2018).
- [16] R.-X. Zhang, W. S. Cole, X. Wu, and S. Das Sarma, *Phys. Rev. Lett.* **123**, 167001 (2019).
- [17] M. Bazarnik, R. L. Conte, E. Mascot, K. von Bergmann, D. K. Morr, and R. Wiesendanger, *Nat. Commun.* **14**, 614 (2023).
- [18] V. Mourik, K. Zuo, S. M. Frolov, S. Plissard, E. P. Bakkers, and L. P. Kouwenhoven, *Science* **336**, 1003 (2012).
- [19] A. Das, Y. Ronen, Y. Most, Y. Oreg, M. Heiblum, and H. Shtrikman, *Nat. Phys.* **8**, 887 (2012).
- [20] S. Nadj-Perge, I. K. Drozdov, J. Li, H. Chen, S. Jeon, J. Seo, A. H. MacDonald, B. A. Bernevig, and A. Yazdani, *Science* **346**, 602 (2014).
- [21] J.-P. Xu, M.-X. Wang, Z. L. Liu, J.-F. Ge, X. Yang, C. Liu, Z. A. Xu, D. Guan, C. L. Gao, D. Qian, Y. Liu, Q.-H. Wang, F.-C. Zhang, Q.-K. Xue, and J.-F. Jia, *Phys. Rev. Lett.* **114**, 017001 (2015).
- [22] G. C. Ménard, S. Guissart, C. Brun, R. T. Leriche, M. Trif, F. Debontridder, D. Demaille, D. Roditchev, P. Simon, and T. Cren, *Nat. Commun.* **8**, 2040 (2017).
- [23] J. Chen, P. Yu, J. Stenger, M. Hocevar, D. Car, S. R. Plissard, E. P. A. M. Bakkers, T. D. Stanescu, and S. M. Frolov, *Sci. Adv.* **3**, e1701476 (2017).
- [24] D. Wang, L. Kong, P. Fan, H. Chen, S. Zhu, W. Liu, L. Cao, Y. Sun, S. Du, J. Schneeloch, R. Zhong, G. Gu, L. Fu, H. Ding, and H.-J. Gao, *Science* **362**, 333 (2018).
- [25] S. Kezilebieke, M. N. Huda, V. Vaño, M. Aapro, S. C. Ganguli, O. J. Silveira, S. Głodzik, A. S. Foster, T. Ojanen, and P. Liljeroth, *Nature* **588**, 424 (2020).
- [26] S. Vaitiekėnas, Y. Liu, P. Krogstrup, and C. M. Marcus, *Nat. Phys.* **17**, 43 (2020).
- [27] S. Manna, P. Wei, Y. Xie, K. T. Law, P. A. Lee, and J. S. Moodera, *Proc. Natl. Acad. Sci.* **117**, 8775 (2020).
- [28] Z. Liang, X. Hou, F. Zhang, W. Ma, P. Wu, Z. Zhang, F. Yu, J.-J. Ying, K. Jiang, L. Shan, Z. Wang, and X.-H. Chen, *Phys. Rev. X* **11**, 031026 (2021).
- [29] J. Liu, A. C. Potter, K. T. Law, and P. A. Lee, *Phys. Rev. Lett.* **109**, 267002 (2012).
- [30] D. I. Pikulin, J. P. Dahlhaus, M. Wimmer, H. Schomerus, and C. W. J. Beenakker, *New J. Phys.* **14**, 125011 (2012).
- [31] C. Moore, C. Zeng, T. D. Stanescu, and S. Tewari, *Phys. Rev. B* **98**, 155314 (2018).
- [32] J. Chen, B. D. Woods, P. Yu, M. Hocevar, D. Car, S. R. Plissard, E. P. A. M. Bakkers, T. D. Stanescu, and S. M. Frolov, *Phys. Rev. Lett.* **123**, 107703 (2019).
- [33] A. Vuik, B. Nijholt, A. Akhmerov, and M. Wimmer, *SciPost Phys.* **7**, 061 (2019).
- [34] J. Jünger, R. Delagrangé, D. Chevallier, S. Lehmann, K. A. Dick, C. Thelander, J. Klinovaja, D. Loss, A. Baumgartner, and C. Schönenberger, *Phys. Rev. Lett.* **125**, 017701 (2020).
- [35] E. Prada, P. San-Jose, M. W. A. de Moor, A. Geresdi, E. J. H. Lee, J. Klinovaja, D. Loss, J. Nygård, R. Aguado, and L. P. Kouwenhoven, *Nat. Rev. Phys.* **2**, 575 (2020).
- [36] H. Pan and S. D. Sarma, *Phys. Rev. Research* **2**, 013377 (2020).
- [37] S. D. Sarma and H. Pan, *Phys. Rev. B* **103**, 195158 (2021).
- [38] D. Sticlet, C. Bena, and P. Simon, *Phys. Rev. Lett.* **108**, 096802 (2012).
- [39] J. J. He, T. K. Ng, P. A. Lee, and K. T. Law, *Phys. Rev. Lett.* **112**, 037001 (2014).
- [40] A. Haim, E. Berg, F. von Oppen, and Y. Oreg, *Phys. Rev. Lett.* **114**, 166406 (2015).
- [41] H.-H. Sun, K.-W. Zhang, L.-H. Hu, C. Li, G.-Y. Wang, H.-Y. Ma, Z.-A. Xu, C.-L. Gao, D.-D. Guan, Y.-Y. Li, C. Liu, D. Qian, Y. Zhou, L. Fu, S.-C. Li, F.-C. Zhang, and J.-F. Jia, *Phys. Rev. Lett.* **116**, 257003 (2016).
- [42] L.-H. Hu, C. Li, D.-H. Xu, Y. Zhou, and F.-C. Zhang, *Phys. Rev. B* **94**, 224501 (2016).
- [43] S. Jeon, Y. Xie, J. Li, Z. Wang, B. A. Bernevig, and A. Yazdani, *Science* **358**, 772 (2017).
- [44] D. Wang, J. Wiebe, R. Zhong, G. Gu, and R. Wiesendanger, *Phys. Rev. Lett.* **126**, 076802 (2021).
- [45] B. Jäck, Y. Xie, and A. Yazdani, *Nat. Rev. Phys.* **3**, 541 (2021).
- [46] X. Liu, J. D. Sau, and S. D. Sarma, *Phys. Rev. B* **92**, 014513 (2015).
- [47] K. Zhang, J. Zeng, Y. Ren, and Z. Qiao, *Phys. Rev. B* **96**, 085117 (2017).
- [48] N. F. Q. Yuan, Y. Lu, J. J. He, and K. T. Law, *Phys. Rev. B* **95**, 195102 (2017).
- [49] W.-Y. He, B. T. Zhou, J. J. He, N. F. Yuan, T. Zhang, and K. T. Law, *Commun. Phys.* **1**, 40 (2018).
- [50] J. Li, T. Neupert, Z. Wang, A. H. MacDonald, A. Yazdani, and B. A. Bernevig, *Nat. Commun.* **7**, 12297 (2016).
- [51] S. Rachel, E. Mascot, S. Cocklin, M. Vojta, and D. K. Morr, *Phys. Rev. B* **96**, 205131 (2017).
- [52] See Supplementary Materials at [this page](#) for more details on model construction, pairing correlation for typical minimal models of TSC, and comments on methods for transport calculations, which includes Refs. [57–61].
- [53] L. P. Gor'kov and E. I. Rashba, *Phys. Rev. Lett.* **87**, 037004 (2001).
- [54] F. Crépin, P. Burset, and B. Trauzettel, *Phys. Rev. B* **92**, 100507 (2015).
- [55] T. Kieu, E. Mascot, J. Bedow, R. Wiesendanger, and D. K. Morr, *Phys. Rev. B* **108**, L060509 (2023).

- [56] R. S. Keizer, S. T. B. Goennenwein, T. M. Klapwijk, G. Miao, G. Xiao, and A. Gupta, *Nature* **439**, 825 (2006).
- [57] P. A. Lee and D. S. Fisher, *Phys. Rev. Lett.* **47**, 882 (1981).
- [58] S. Datta, *Electronic Transport in Mesoscopic Systems*, edited by H. Ahmed, M. Pepper, and A. Broers, Cambridge Studies in Semiconductor Physics and Microelectronic Engineering No. 3 (World Publishing Corporation, Beijing, 2004).
- [59] Z. Qiao and J. Wang, *Nanotechnol.* **18**, 435402 (2007).
- [60] M. G. Reuter, T. Seideman, and M. A. Ratner, *Phys. Rev. B* **83**, 085412 (2011).
- [61] L. R. F. Lima, A. Dusko, and C. Lewenkopf, *Phys. Rev. B* **97**, 165405 (2018).